Journal of Molecular Catalysis A: Chemical 348 (2011) 100–105

Contents lists available at SciVerse ScienceDirect

Journal of Molecular Catalysis A: Chemical

journal homepage: www.elsevier.com/locate/molcata

Photocatalytic activity and photoelectric performance enhancement for $ZnWO_4$ by fluorine substitution

Guangli Huang[a,b], Rui Shi[a], Yongfa Zhu[a,*]

[a] Department of Chemistry, Tsinghua University, Beijing 100084, PR China
[b] Beijing Tobacco Quality Supervision and Test Station, Beijing 100029, PR China

ARTICLE INFO

Article history:
Received 7 March 2011
Received in revised form 19 July 2011
Accepted 16 August 2011
Available online 24 August 2011

Keywords:
Photocatalyst
$ZnWO_4$
Fluorine substitution

ABSTRACT

The formation of fluorine substitution on $ZnWO_4$ ($ZnWO_{4-x}F_{2x}$) can be easily attained by a two step process. It could be speculated that oxygen ion was substituted by fluorine ion in the crystal lattice of $ZnWO_4$ on the basis of XPS and IR results. Comparing with $ZnWO_4$, the photocatalytic activity of $ZnWO_{4-x}F_{2x}$ sample almost doubled for degradation of methylene blue under UV irradiation. The enhanced photocatalytic activity should be attributed to higher density of surface hydroxyl groups of $ZnWO_{4-x}F_{2x}$ which induced $OH^{\bullet}$ radicals to improve photocatalytic reaction. Additionally, $ZnWO_{4-x}F_{2x}$ possessed higher donor density and efficiency of charge separation to increase the transfer rate of charges to the photocatalyst surface and to promote photocatalytic reaction.

1. Introduction

Semiconductor photocatalytic processes have been widely applied as techniques of destruction of organic pollutants in wastewater [1,2]. Recently, some tungstates such as Bi_2WO_6 and $ZnWO_4$ have presented high photoactivities for the pollutant degradation [3–5]. Their unique combination of physical and chemical properties, in terms of molecular and electronic versatility, reactivity, and stability, make us believe they are fine photocatalytic candidate materials. Therefore, further improving their photocatalytic activity for practical application is significant and meaningful.

In these years, fluorine ion acting as promising dopants in TiO_2 had attracted a great deal of attention [6–10]. TiO_2 photocatalyst after being doped by fluorine exhibit greater enhanced photocatalytic activity than before. The mechanisms of enhanced photocatalytic activities follow several ways: (1) Doping fluorine ion convert Ti^{4+} to Ti^{3+} by charge compensation and presence of a certain amount of Ti^{3+} reduce the electron-hole recombination rate [6]. (2) Fluorine doping induce homogeneous free $OH^{\bullet}$ radicals to promote photocatalytic reaction [7,8]. (3) Fluorine doping result in the increase in anatase crystallinity [9], etc.

Very recently, a few fluorine doped non-TiO_2 catalysts also exhibited a similar enhancement of photocatalytic activities. Fluorine doped $SrTiO_3$ showed about three times the photocatalytic activity compared with that of undoped $SrTiO_3$ [11]. The enhancement of photocatalytic activity was mainly ascribable to the formation of oxygen vacancies and increase of effective electron mobility. Additionally, enhanced photocatalytic activity on Bi_2WO_6 and $ZnWO_4$ by fluorine introduction was reported by our and the other groups [12–15]. Our preliminary experiments demonstrated that the improved photocatalytic activity by interstitial F impurity was ascribed to an increase of the transfer-rate of photogenerated electrons to the surface of photocatalyst [13]. In this work, we want to know whether the photocatalytic mechanism is different between F substitution and F interstitial doped $ZnWO_4$.

We reported herein the photocatalytic performance of fluorine substituted $ZnWO_4$ ($ZnWO_{4-x}F_{2x}$) prepared by a two-step process. To our knowledge, the effects of fluorine substitution and heat treatment on the photocatalytic activity of $ZnWO_4$ have not been reported. In this study, we investigated the effects of fluorine on photoelectric behavior and photocatalytic reaction of $ZnWO_4$. The results gained in this study are helpful for understanding the mechanism in the F substituted O-doped $ZnWO_4$, which also show promising photocatalytic activity.

2. Experimental

2.1. Synthesis of substituted sample

$ZnWO_{4-x}F_{2x}$ samples were prepared by a two-step process. All chemicals used were analytic grade reagents, without further purification. The starting materials of 0.01 mol Na_2WO_4 and 30 mL hydrofluoric acid were stirred and heated, thus, forming $Na_2WO_2F_4$ compound (see Supporting Information Fig. S1). In what followed, the $Na_2WO_2F_4$ and Zn $(NO_3)_2$ were soaked in water in a stoichiometric ratio, refluxed on a mantle heater for 24 h. The products

* Corresponding author.
E-mail address: zhuyf@mail.tsinghua.edu.cn (Y. Zhu).

1381-1169/$ – see front matter © 2011 Elsevier B.V. All rights reserved.
doi:10.1016/j.molcata.2011.08.013

were washed with water and filtered. The obtained precursors were dried at 333 K. In order to improve crystallinity of $ZnWO_{4-x}F_{2x}$, the obtained samples were annealed at several temperatures for 1 h in a crucible in air. Meanwhile $ZnWO_4$ samples were synthesized by the same method for comparison with the $ZnWO_{4-x}F_{2x}$ samples.

2.2. Characterization

Purity and crystallinity of the as-prepared sample was characterized by XRD on Bruker D8-advance diffractometer using Cu Kα radiation. The XRD data for indexing and cell-parameter calculation were collected in a scanning mode with a step length of 0.02° and a preset time of 1 s/step. Thermogravimetric analysis (TGA) and differential thermal analysis (DTA) were performed on a Dupont 1090 thermal analyzer, the atmosphere was air, and the heating rate was 5 °C min^{-1}. Chemical characterization of the sample surface was recorded with X-ray photoelectron spectroscopy (XPS ULVAC-PHI, Quantera). The charging effect was calibrated using the binding energy of C 1s. Fourier transform infrared spectra (FT-IR) were recorded on a Perkin-Elmer 1600 FT-IR spectrometer with a KBr disk. Diffuse reflection spectra (DRS) were obtained on a Hitachi U-3010 UV–vis spectrophotometer.

2.3. Photocatalytic tests and photoelectrochemical performance

The photocatalytic activities of the $ZnWO_{4-x}F_{2x}$ and $ZnWO_4$ were evaluated by degradation of methylene blue (MB) under UV light irradiation of an 11 W low-pressure lamp with 254 nm. The average light intensity was 0.9 mW/cm^2. The radiant flux was measured with a power meter from the Institute of Electric Light Source (Beijing). MB solution (100 mL, 1.0×10^{-5} mol L^{-1}) containing 50 mg of as-prepared samples were placed in a glass beaker. Before the light was turned on, the solution was stirred for 30 min to ensure equilibrium between the catalysts. 3 mL of sample solution were taken at given time intervals and separated through centrifugation. The changes of MB concentration were monitored by the variations in absorption intensity at 663 nm using a UV–vis spectrometer (Hitachi U-3010). The photoelectrochemical studies were performed on a CHI 660B electrochemical system (Shanghai, China) using a standard three-electrode cell with a working electrode, a platinum wire counter electrode, and a standard calomel electrode (SCE) reference electrode. The working electrodes were prepared by dip-coating: briefly, 5 mg of photocatalyst was suspended in 3 mL water to produce slurry, which was then dip-coated on a 20 mm × 40 mm indium–tin oxide (ITO) glass electrode. Electrodes were exposed to UV light for 3 days to eliminate water and subsequently dried at 353 K for 2 days. All investigated working electrodes were of similar thickness (0.1–0.12 mm). Photoelectrochemical properties were measured with an 18 W germicidal lamp with 254 nm. Unless otherwise stated, the intensity of light at the film electrode was 1.5 mW/cm^2 at the wavelength of 254 nm, and 0.1 M Na_2SO_4 electrolytes were used. The electrochemical impedance spectroscopy (EIS) was carried out at the open circuit potential. A sinusoidal ac-perturbation of 5 mV was applied to electrode over the frequency range of 0.05–10^5 Hz.

3. Results and discussion

3.1. Chemical states of fluorine

Fig. 1 shows XRD pattern of $ZnWO_{4-x}F_{2x}$ obtained at different annealing temperature. It illustrates that fluorine substitution did not result in the development of new crystal orientations or changes in preferential orientations. This result is agreement with the quantum mechanical study by Fan groups, which confirmed that the whole structural variations following O replacement with

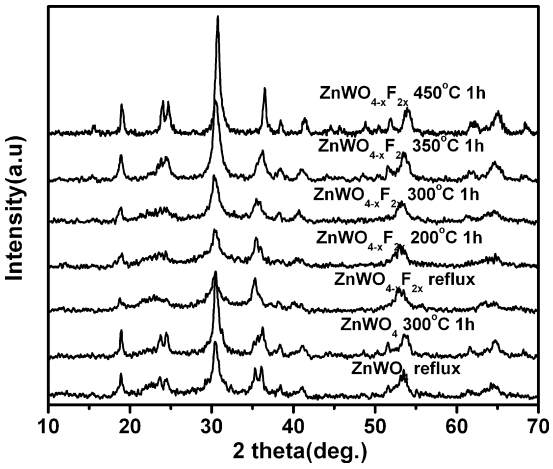

Fig. 1. X-ray diffraction pattern of $ZnWO_4$ and $ZnWO_{4-x}F_{2x}$ annealed at several temperature.

F were found to be slight [16]. Hence, independently of presence or absence of fluorine, the samples appeared to be phase-pure monoclinic $ZnWO_4$ phase [JCPDS No. 15-0774]. This result was also agreement with the F substituted O-doped Bi_2WO_6, which claimed that F substitution did not result in the changes of composition of pure orthorhombic Bi_2WO_6 phase [12]. However, a careful comparison between the diffraction peaks of $ZnWO_4$ and $ZnWO_{4-x}F_{2x}$ prepared at same condition showed the crystallization of $ZnWO_4$ was better than that of $ZnWO_{4-x}F_{2x}$, which would be due to the pH value in the reaction system. $Na_2WO_2F_4$ came from Na_2WO_4 and hydrofluoric acid. So there must be lots of HF molecules existing in interstitial lattice and on the surface of $Na_2WO_2F_4$. Obviously, the pH value of the precursor medium of $ZnWO_{4-x}F_{2x}$ was very low. According to Ref. [17], the optimal pH value for the formation of $ZnWO_4$ was in the range of pH value 6–11. Hence, the crystallization of $ZnWO_{4-x}F_{2x}$ was worse than that of $ZnWO_4$ under the same conditions.

In order to explore the thermal stability of reflux precursor of $ZnWO_{4-x}F_{2x}$ and $ZnWO_4$ in the air, the possible gravimetric and thermal changes were investigated by TG and DTA (Fig. 2). It can be found from the TG curve (Fig. 2A) that the increase of temperature resulted in weight loss (about 7.8%). The weight loss region from 45 to 450 °C was caused by the loss of coordinated water. One endothermic peak was observed on the DTA curve (Fig. 2A). The peak at 416 °C could be assigned to the formation of $ZnWO_4$ complicated oxide [18]. However, the DTA and TG curve of $ZnWO_{4-x}F_{2x}$ reflux precursor was different from $ZnWO_4$ reflux precursor (Fig. 2B). The weight loss about 6.6% from 45 to 450 °C was caused by the loss of coordinated water and fluorine of chemical absorption. The weight loss about 1.2% from 450 °C to 610 °C may be caused by the loss of coordinated fluorine. The endothermic peak at 426 °C could be assigned to the formation of $ZnWO_{4-x}F_{2x}$ complicated oxide [18]. It illustrated that temperature of phase formation increased after F substituted O-doped $ZnWO_4$. The peak at 660 °C resulted from the further crystallization of $ZnWO_{4-x}F_{2x}$. Finally, the peak at 870 °C could be interpreted as the formation of new phase.

Fig. 3A shows the XPS survey spectrum of $ZnWO_{4-x}F_{2x}$ and $ZnWO_4$. It was clear that $ZnWO_{4-x}F_{2x}$ synthesized only by reflux method was mainly composed of Zn, W, O and F elements and a trace amount of carbon. Quantitative analysis demonstrated that the atomic ratio of F/Zn was 0.25. However, the atomic ration of F/Zn was 0.2 after this sample was annealed at 300 °C for 1 h. Therefore, the increase in annealing temperature would correspond to a decrease of fluorine content, which was consistent with the results of TGA and DTA. Comparing with $ZnWO_{4-x}F_{2x}$, there was no

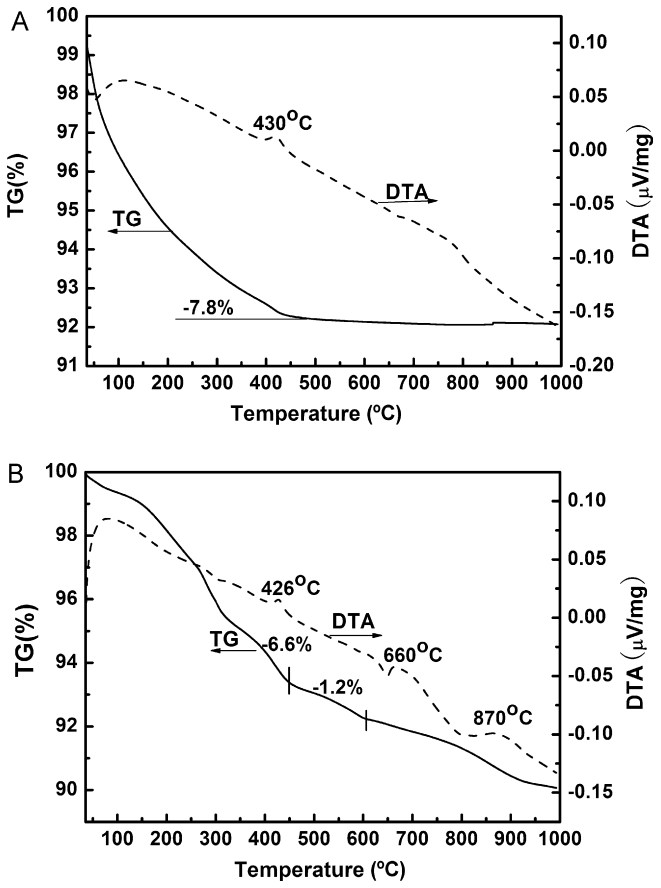

Fig. 2. TG and DTA analysis of reflux precursor of $ZnWO_4$ (A) and $ZnWO_{4-x}F_{2x}$ (B).

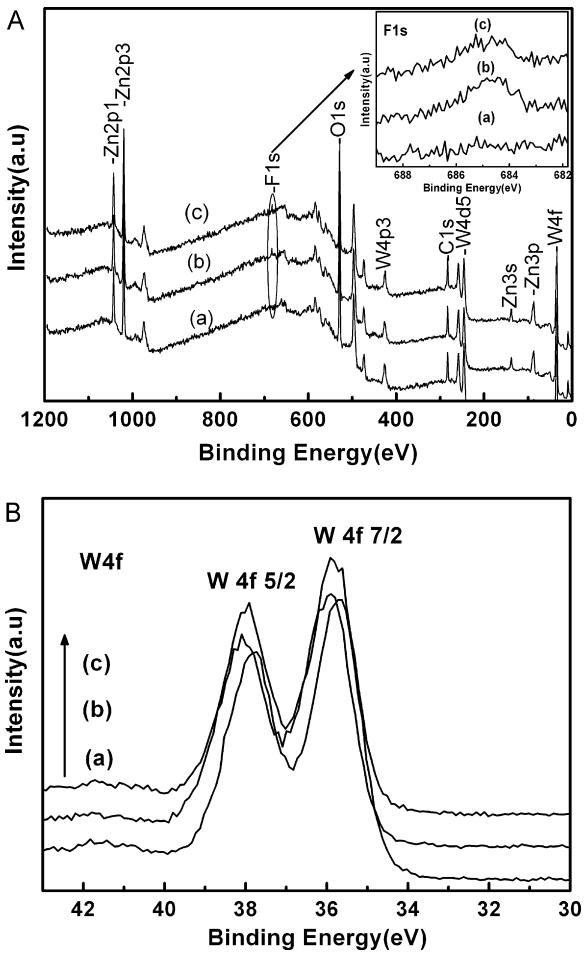

Fig. 3. X-ray photoelectron survey (A) and narrow (B) spectrum: (a) $ZnWO_4$ reflux; (b) $ZnWO_{4-x}F_{2x}$ reflux; (c) $ZnWO_{4-x}F_{2x}$ annealed at 300 °C.

fluorine trace in $ZnWO_4$. An XPS spectrum of F 1s peaks were shown in the inset of Fig. 3A. The banding energy of F 1s was 684.7 eV. Generally, the F 1s binding energy of 684 eV corresponds to the fluorine ions adsorbed on the TiO_2, and that of 688 eV corresponds to the fluorine ion in the lattice [6,19]. And in our recently work, our group demonstrated the F 1s binding energy of 684.1 eV in $ZnWO_4$–F can be assigned to the contribution of fluorine ions in the interstitial lattice of $ZnWO_4$ crystal [13]. However, according to the results of $Cs_2WO_2F_4$, the binding energy of F 1s is 684.7 eV [20], which is consistent with that of fluorine in $ZnWO_{4-x}F_{2x}$. Hence, the XPS results displayed that the fluorine ion substituted for oxygen ion in $ZnWO_4$ cell. In order to further confirm this conclusion, chemical environment surrounding the W elements in $ZnWO_{4-x}F_{2x}$ was investigated, and $ZnWO_4$ was selected as a standard for XPS measurement. W 4f XPS results of $ZnWO_{4-x}F_{2x}$ and $ZnWO_4$ are shown in Fig. 3B. The binding energies were 38.0 and 35.8 eV, respectively, for W 4f5/2 and W 4f7/2 in the oxide form of $ZnWO_4$, which could be characteristic of W element in the WO_6 octahedron. However, for $ZnWO_{4-x}F_{2x}$, the binding energy of the peak of W 4f5/2 and W 4f7/2 increased about 0.2 eV, which was attributed to the change of the chemical environment surrounding W. Some mixed states such as F–W–O may be the case, which supported that fluorine ion substituted for oxygen ion. Note that the same result was obtained in the F substituted Bi_2WO_6 [12].

Fig. 4 shows FT-IR spectra of $ZnWO_4$ and $ZnWO_{4-x}F_{2x}$ annealed at 300 °C. The bands at 3300–3600 cm^{-1} were attributed to OH stretching vibration, and the band at 1620 cm^{-1} was attributed to the bending mode of OH groups. We could see that the intensities of $ZnWO_{4-x}F_{2x}$ was stronger than that of $ZnWO_4$ in the same synthesis condition, indicating the number of surface hydroxyl groups of $ZnWO_{4-x}F_{2x}$ was more than that of $ZnWO_4$. The peaks in the range of 900–400 cm^{-1} assigned to the stretching vibrations of $ZnWO_4$ [21,22]. In the FT-IR spectra of $ZnWO_4$, the banding and stretching vibration of Zn–O occurred at 432 and 463 cm^{-1}. The bands corresponding to W–O bond stretching and bending vibrations in WO_6 group occurred at 815, 711 and 618 cm^{-1}. This indicated the good crystallinity and relatively low concentration of defects in $ZnWO_4$. However, as for $ZnWO_{4-x}F_{2x}$, the bands at 463 and 432 cm^{-1} was related to vibrations of Zn–O bond, the

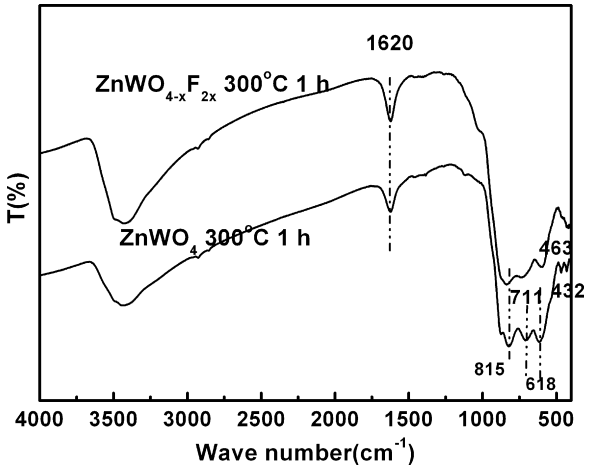

Fig. 4. FT-IR spectra of $ZnWO_4$ and $ZnWO_{4-x}F_{2x}$ annealed at 300 °C.

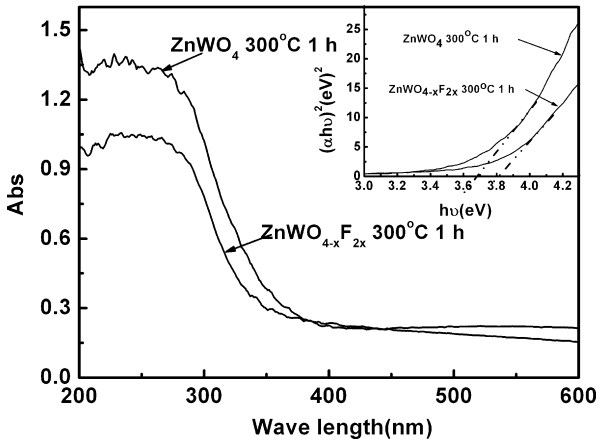

Fig. 5. UV–vis diffuse reflectance spectra of $ZnWO_4$ and $ZnWO_{4-x}F_{2x}$ annealed at 300 °C.

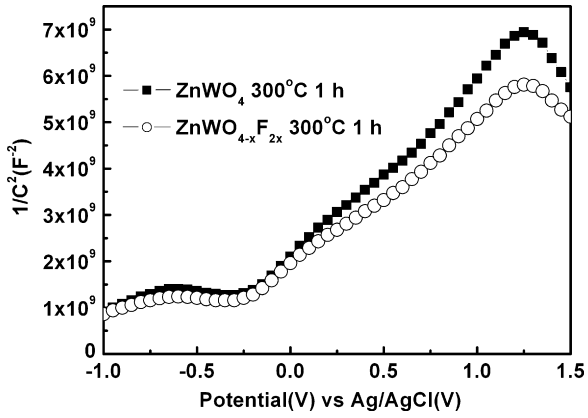

Fig. 6. Mott–Schottky (MS) plots of $ZnWO_4$ and $ZnWO_{4-x}F_{2x}$ annealed at 300 °C thin film electrodes.

intensities of which decreased with fluorine ion substituting with oxygen ion. This implied Zn–O bond could be reduced and Zn–F bond could be formed. Moreover, compared with the W–O band of $ZnWO_4$ at 618 cm^{-1} (WO_6 octahedron stretching mode), the band of $ZnWO_{4-x}F_{2x}$ shifted to 601 cm^{-1}. According to reference, the vibration of W–F band located at 601 cm^{-1} [23]. For the F substituted O-doped $ZnWO_4$ structure, the two F–W bonds are stretched to 2.065 and 2.269 Å compared with the original O–W bonds 1.919 and 2.158 Å [17]. The increase of the bond length could also result in the shift from 618 cm^{-1} to 601 cm^{-1}. Therefore, combining with XPS data, fluorine ion must substitute for oxygen ion in $ZnWO_{4-x}F_{2x}$.

3.2. Effect of fluorine substitution on photoelectric properties

DRS of the $ZnWO_4$ and $ZnWO_{4-x}F_{2x}$ annealed at 300 °C are shown in Fig. 5. It was noteworthy that the absorption onset of $ZnWO_{4-x}F_{2x}$ was blue-shifted apparently. The value of band gap for $ZnWO_4$ and $ZnWO_{4-x}F_{2x}$ were determined as 3.68 and 3.81 eV by extrapolation method, respectively (see inset in Fig. 5). Furthermore, $ZnWO_{4-x}F_{2x}$ sample presented weaker absorption than $ZnWO_4$ in the UV range. The absorption of $ZnWO_4$ under UV regions was assigned to the band transition from the occupied O 2p orbital to the empty W 5d orbital [24]. On the basis of the XRD, XPS and IR results, F ion occupy the O position, because F^- and O^{2-} ions have the same electronic configuration, and nearly the same ionic radius (0.136 and 0.144 nm for F^- and O^{2-}, respectively). Therefore, significant hybridization of the 2p states of F and the 2p states of O may be exist in $WO_{6-x}F_{2x}$ octahedron [25]. Consequently, this transition in $WO_{6-x}F_{2x}$ octahedron required a higher energy than the transition in WO_6 octahedron owing to larger electronegativity of fluorine. The broadening band gap of $ZnWO_{4-x}F_{2x}$ could testify this conclusion. Moreover, this conclusion was similar to the result of fluorine-doped TiO_2 reported by Hattori and Tada [26], who claimed that doped fluorine contributed to the charge-transfer transition of TiO_2.

In order to better understand the differences in the photoelectric properties of $ZnWO_4$ and $ZnWO_{4-x}F_{2x}$, their electrode were examined under various electrochemical conditions. Fig. 6 shows Mott–Schottky (MS) plots, $1/C^2$ versus E, for the $ZnWO_4$ and $ZnWO_{4-x}F_{2x}$ annealed at 300 °C. Reversed sigmoidal plots were observed with an overall shape that was consistent with that of typical n-type semiconductors. The intersection point of the potential and linear potential curves gave a flat band potential, which in this case was approximately −0.57 and −0.60 V versus Ag/AgCl for $ZnWO_4$ and $ZnWO_{4-x}F_{2x}$, respectively. $ZnWO_{4-x}F_{2x}$ experienced a negative shift of the flat-band potential when compared with $ZnWO_4$. It is generally known that the conduction band minimum (CBM) in many n-type semiconductors is more negative by approximately −0.1 V than the flat band potential [27,28]. According to the value of band gap (DRS result), the estimated positions of valence band maximum (VBM) were 3.21 and 3.31 V versus Ag/AgCl, respectively, for $ZnWO_4$ and $ZnWO_{4-x}F_{2x}$. The VBM of $ZnWO_{4-x}F_{2x}$ was lowered from those of $ZnWO_4$ by 0.1 V. The lowering of the VBM indicated that $ZnWO_{4-x}F_{2x}$ had a stronger oxidation power theoretically. Additionally, it was noteworthy that the slope of the linear region for $ZnWO_{4-x}F_{2x}$ electrode was lower in value, which suggested a higher donor density. For n-type semiconductors electrode, it was shown that donor density follows the equation (reaction (1)) [29]:

$$\frac{1}{C^2} = \left(\frac{2}{eN_d \in_0 \in}\right)|V - V_{fb}| \quad (1)$$

where N_d is the donor density (cm^{-3}), e is the electronic charge unit, ε_0 is the permittivity of free space, ε is the dielectric constant, V is the applied potential (V), and V_{fb} is the flat-band potential (V). It shows that when $1/C^2$ is zero, the x-intercept is equal to the flat band potential V_{fb}, so the calculated donor density N_d was 2.36×10^{19} and 3.01×10^{19} cm^{-3}, respectively, for $ZnWO_4$ and $ZnWO_{4-x}F_{2x}$.

According to the reference, effects of fluorination could reduce the electron–hole recombination rate [19]. Yu et al. proposed that TiO_2 surface fluorination group seemed to act as electron-trapping site, inhibit interfacial electron–hole recombination and enhance photocatalytic degradation behavior due to the strong electronegativity of the fluorine [6]. To investigate the influence of fluorine substitution on photoelectric property, EIS technology was used to study the solid/electrolyte interfaces of $ZnWO_4$ and $ZnWO_{4-x}F_{2x}$ sample under UV light irradiation (Fig. 7). According to conventional double-layer theories, the electrical double layer at solid electrode behaved as a frequency distribution impedance instead of a pure capacitance due to the surface heterogeneity. When the charge transfer reaction occurred, the Nyquist plot was a semicircle; when semi-infinite diffusion was rate-determining step, a linear with a slope of 45° appeared [30]. In our case, only one semicircle on the EIS plane suggested charge transfer occurring. The diameter of the arc radius on the EIS Nynquist plot of the $ZnWO_{4-x}F_{2x}$ was smaller than that of $ZnWO_4$. The smaller arc radius of the EIS Nynquist plot suggested a higher efficiency of charge separation [31]. Thus, in the case of $ZnWO_{4-x}F_{2x}$, the photoinduced electron–hole pairs were easier separated and transferred to the sample surface. And this result also supported the MS conclusion.

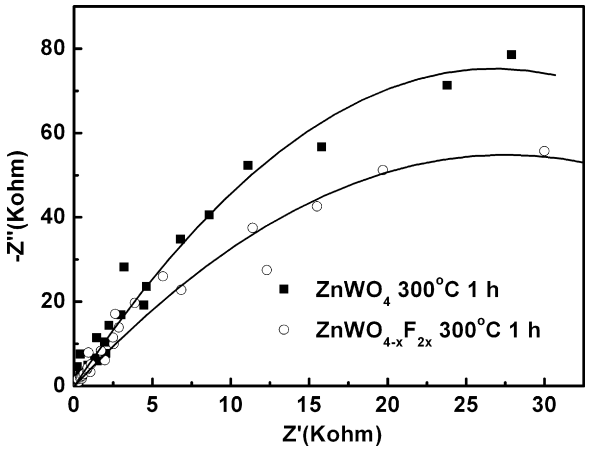

Fig. 7. Impedance spectra of under $ZnWO_4$ and $ZnWO_{4-x}F_{2x}$ annealed at 300 °C thin film electrodes under UV light irradiation.

3.3. Effect of fluorine substitution on photocatalytic activity

The photoactivities of samples were evaluated by degradation of MB, a hazardous solution pollutant as well as a common model compound to test the photodegradation capability of photocatalytsts. Fig. 8 shows the relationship between annealing temperature and reaction constant of MB degradation over $ZnWO_4$ and $ZnWO_{4-x}F_{2x}$. These two samples prepared by reflux method both showed low photocatalytic activities with rate constant of 3.06×10^{-3} min^{-1} and 3.76×10^{-3} min^{-1}, respectively, for $ZnWO_4$ and $ZnWO_{4-x}F_{2x}$. Many studies had shown that annealing was an effective treatment method to enhance the photocatalytic activity. With an increase of annealing temperature, the photocatalytic activity of $ZnWO_{4-x}F_{2x}$ increased. It was notable that the rate of MB decomposition of $ZnWO_{4-x}F_{2x}$ was higher than that of $ZnWO_4$ under the same annealing treatment. At annealing temperature of 350 °C, the rate constant of $ZnWO_{4-x}F_{2x}$ reached the highest value of 1.25×10^{-2} min^{-1}, which was about two times compared with that of $ZnWO_4$. The enhancement of photocatalytic activity of $ZnWO_{4-x}F_{2x}$ at elevated temperature can be ascribed to an obvious improvement in crystallinity and a decrease in lattice defects. However, annealing temperature well above 350 °C was not desirable. When the annealing temperature reached too high, fluorine content would reduce (as shown in TG, DTA and XPS results). And too little fluorine content did not influence the photocatalytic activity of $ZnWO_{4-x}F_{2x}$. Thus, the activity of $ZnWO_{4-x}F_{2x}$ was almost similar to that of $ZnWO_4$ under high annealing temperature

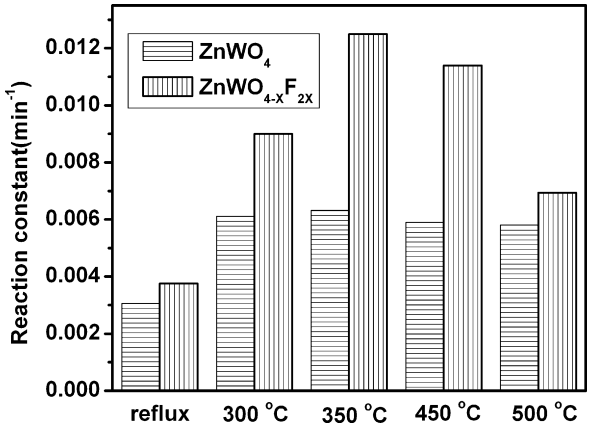

Fig. 8. Photocatalytic degradation MB under UV light irradiation over $ZnWO_4$ and $ZnWO_{4-x}F_{2x}$ annealed at several temperature.

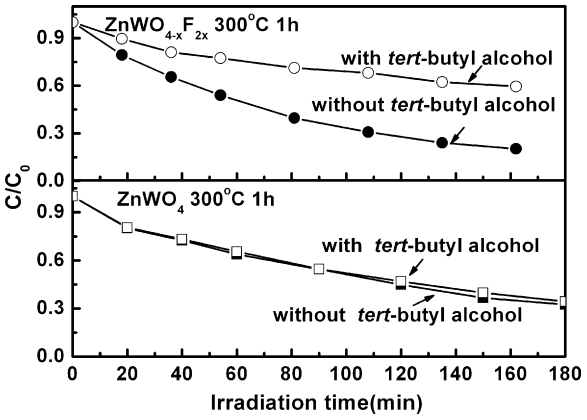

Fig. 9. Effect of *tert*-butyl alcohol addition on the degradation of MB over $ZnWO_4$ and $ZnWO_{4-x}F_{2x}$ annealed at 300 °C. [*tert*-butyl alcohol] = 1 mM.

(500 °C). In order to achieve a high photocatalytic rate, a balance between annealing temperature and fluorine content was required. $ZnWO_{4-x}F_{2x}$ annealed at 350 °C gave the highest rate constant while lattice defects were suppressed and fluorine content was enough to influence photocatalytic activity. $ZnWO_{4-x}F_{2x}$ as a kind of photocatalyst can be easily recycled by a simple filtration. After three recycles for the photodegradation of MB, the photocatalyst did not exhibit any significant loss of activity, as shown in Supporting Information Fig. S2, confirming $ZnWO_{4-x}F_{2x}$ was not photo-corroded during the photocatalytic reaction.

3.4. The mechanism of enhanced photocatalytic activity

On the basis of XPS and IR results, it could be speculated that oxygen ion was substituted by fluorine ion in the crystal lattice of $ZnWO_4$. Thus, the enhanced photocatalytic activity could be assigned to fluorine substitution. According to the IR results, the number of surface hydroxyl groups of $ZnWO_{4-x}F_{2x}$ was more than that of $ZnWO_4$. Generally, surface hydroxyl group are considered as the main factor influencing the photocatalytic activity. They react with photogenerated holes, producing active $OH^\bullet$ radicals [32]. In addition, surface hydroxyl groups can act as surface sites for adsorbing organic molecules, which also efficiently capture photogenerated holes [1]. The trapping of holes stabilizes photogenerated electron–hole pairs, improving photocatalytic efficiency.

For photooxidations occurring in oxygenated, aqueous media, the mechanism may, furthermore, involve direct reaction of the organic chemical (dye) with surface h_{vb}^+, indirect reaction with $OH^\bullet$ radicals, or a dual mechanism involving both surface h_{vb}^+ and $OH^\bullet$ radicals (reaction (2)):

$$h_{vb}^+/OH^\bullet + \text{dye(MB)} \rightarrow \text{products} \quad (2)$$

To study the process of the photooxiation of $ZnWO_{4-x}F_{2x}$, experiments were carried out by adding *tert*-butyl alcohol as $OH^\bullet$ radical scavenger (Fig. 9). The addition of *tert*-butyl alcohol greatly reduced the photodegradation rate of MB in the $ZnWO_{4-x}F_{2x}$ suspension, whereas its addition had little effect on the MB degradation in $ZnWO_4$ suspension. This implied that the MB degradation in $ZnWO_{4-x}F_{2x}$ suspension proceeded through a mechanistic path that was different from that in $ZnWO_4$. The different mechanism between these two systems could be ascribed to the different main oxidant species on the surface of $ZnWO_4$ and $ZnWO_{4-x}F_{2x}$. MB degradation on $ZnWO_4$ seemed to be initiated mostly by the direct h_{vb}^+ transfer, which was consistent with our previous claim [33]. On the other hand, a dual mechanism involving both surface h_{vb}^+ and $OH^\bullet$ radicals was expected in the photocatalytic process of $ZnWO_{4-x}F_{2x}$. Appearance of $OH^\bullet$ radicals was due to $ZnWO_{4-x}F_{2x}$

samples possessing a higher density of surface hydroxyl groups. Thus, it was to be believed that surface hydroxyl groups had the highest efficiency in trapping the photo-generated holes to form $OH^{\bullet}$ radicals. When $ZnWO_4$ was substituted by fluorine, the photocatalytic process was mainly initiated by $OH^{\bullet}$ radicals via which MB degradation on $ZnWO_{4-x}F_{2x}$ can well proceed. Hence, the preferential formation of $OH^{\bullet}$ radicals on $ZnWO_{4-x}F_{2x}$ had been suggested as a cause of increased photoactivity.

Additionally, it is known that the photocatalytic activity of semiconductor material is partly controlled by the surface charges transfer rate. If this condition reaches decent level, surface favors the occurrence of photochemical reaction. On the basis of the results of Figs. 6 and 7, comparing with $ZnWO_4$, $ZnWO_{4-x}F_{2x}$ possessed higher donor density and efficiency of charge separation. This elucidated that fluorine substitution increased the transfer rate of charges to the photocatalyst surface. So the photogenerated charges could easily diffuse from the inner regions to the surface to promote photocatalytic reaction. Hence, the higher photocatalytic oxidation rate had been ascribed to the higher transfer rate of h_{vb}^{+} and generation of $OH^{\bullet}$ radicals.

4. Conclusions

Fluorine substitution $ZnWO_4$ ($ZnWO_{4-x}F_{2x}$) sample was prepared by a two-step process. Fluorine substitution affected not only the photoelectric properties but also the photocatalytic activity of $ZnWO_4$. The enhancement of photocatalytic activity could be attributed to the increasing in number of surface hydroxyl groups, and higher donor density and efficiency of charge separation caused by fluorine substitution. The photodegradation of MB in $ZnWO_{4-x}F_{2x}$ system mainly proceeded via indirect reaction with $OH^{\bullet}$ radicals.

Acknowledgements

This work is supported by National Natural Science Foundation of China (20925725 and 50972070) and National Basic Research Program of China (2007CB613303).

Appendix A. Supplementary data

Supplementary data associated with this article can be found, in the online version, at doi:10.1016/j.molcata.2011.08.013.

References

[1] M. Hoffmann, S. Martin, M. Choi, D. Banhnemann, Chem. Rev. 95 (1995) 69.
[2] X. Tao, W. Ma, T. Zhang, J. Zhao, Angew. Chem. Int. Ed. 40 (2001) 3014.
[3] C. Zhang, Y. Zhu, Chem. Mater. 17 (2005) 3537.
[4] H. Fu, C. Pan, W. Yao, Y. Zhu, J. Phys. Chem. B 109 (2005) 22432.
[5] J. Lin, J. Lin, Y. Zhu, Inorg. Chem. 46 (2007) 8372.
[6] J. Yu, J. Yu, W. Ho, Z. Jiang, L. Zhang, Chem. Mater. 14 (2002) 3808.
[7] C. Minero, G. Mariella, V. Maurino, E. Pelizzetti, Langmuir 16 (2000) 2632.
[8] C. Minero, G. Mariella, V. Maurino, D. Vione, E. Pelizzetti, Langmuir 16 (2000) 8964.
[9] A. Hattori, M. Yamamoto, H. Tada, S. Ito, Langmuir 15 (1999) 5422.
[10] M. Vohra, S. Kim, W. Choi, J. Photochem. Photobiol. A 160 (2003) 55.
[11] J. Wang, S. Yin, Q. Zhang, F. Saito, T. Sato, J. Mater. Chem. 13 (2003) 2348.
[12] R. Shi, G. Huang, J. Lin, Y. Zhu, J. Phys. Chem. C 113 (2009) 19633.
[13] G. Huang, Y. Zhu, J. Phys. Chem. C 111 (2007) 11952.
[14] S. Chen, S. Sun, H. Sun, W. Fan, X. Zhao, X. Sun, J. Phys. Chem. C 114 (2010) 7680.
[15] H. Fu, S. Zhang, T. Xu, Y. Zhu, J. Chen, Environ. Sci. Technol. 42 (2008) 2085.
[16] H. Sun, W. Fan, Y. Li, X. Cheng, P. Li, X. Zhao, J. Solid State Chem. 183 (2010) 3052.
[17] B. Liu, S. Yu, L. Li, F. Zhang, Q. Zhang, M. Yoshimura, P. She, J. Phys. Chem. B 108 (2004) 2788.
[18] G. Huang, C. Zhang, Y. Zhu, J. Alloys Compd. 432 (2007) 269.
[19] H. Park, W. Choi, J. Phys. Chem. B 108 (2004) 4086.
[20] V. Nefedov, Y. Kokunvo, T. Buslaev, Zh. Neorg, Khim 18 (1973) 931.
[21] J. Lesne, P. Caillet, J. Spectrosc. 18 (1973) 69.
[22] V. Formichev, O. Kondratov, Spectrochim. Acta 50A (1994) 1113.
[23] Y. Katayama, R. Hagiwara, Y. Ito, J. Fluorine Chem. 74 (1995) 89.
[24] H. Fu, J. Lin, L. Zhang, L.Y. Zhu, Appl. Catal. A: Gen. 306 (2006) 58.
[25] X. Liu, G. Hu, X. Feng, Y. Huang, Y. Zhang, Phys. Stat. Sol. (a) 190 (2002) R1.
[26] A. Hattori, H. Tada, J. Sol–Gel Sci. Technol. 22 (2001) 47.
[27] Y. Matsumoto, J. Solid State Chem. 126 (1996) 227.
[28] Y. Matsumoto, K. Omae, I. Watanabe, E. Sato, J. Electrochem. Soc. 133 (1986) 711.
[29] G. Wang, Q. Wang, W. Lu, J. Li, J. Phys. Chem. B 110 (2006) 22029.
[30] J. Li, L. Zheng, L. Li, Y. Xian, L. Jin, J. Hazard. Mater. 139 (2007) 72.
[31] L. Zhang, H. Fu, Y. Zhu, Adv. Funct. Mater. 18 (2008) 2180.
[32] X. Fu, L. Clark, Q. Yang, M. Anderson, Environ. Sci. Technol. 30 (1996) 647.
[33] G. Huang, S. Zhang, T. Xu, Y. Zhu, Environ. Sci. Technol. 42 (2008) 8516.